Distorted Cubane $[Mn_4O_3Cl]^{6+}$ Complexes with Arenecarboxylate Ligation: Crystallographic, Magnetochemical, and Spectroscopic Characterization

Michael W. Wemple,[1a] Hui-Lien Tsai,[2] Kirsten Folting,[1b] David N. Hendrickson,*[,2] and George Christou*[,1a]

Department of Chemistry and Molecular Structure Center, Indiana University, Bloomington, Indiana 47405, and Department of Chemistry—0506, University of California at San Diego, La Jolla, California 92093-0506

Received October 20, 1992

Synthetic procedures are described that allow access to $Mn_4O_3Cl_4(O_2CR)_3(py)_3$ (R = aryl) complexes, complementing previous work with R = alkyl. Carboxylate exchange of the R = Me complex (**2**) with the appropriate arenecarboxylic acid leads to preparation of the R = 3,5-Cl_2-Ph (**3**), Ph (**4**), 4-F-Ph (**5**), and 3,5-F_2-Ph (**6**) complexes. The crystal structure of **3** shows the $[Mn_4O_3Cl]^{6+}$ core to be essentially superimposable on that of **2**. Crystal data for **3** at −171 °C are as follows: hexagonal, $R\bar{3}$, a = 19.056(4) Å, c = 28.271(6) Å, V = 8888.25 Å^3, Z = 6, R (R_w) = 0.0417 (0.0384) employing 1982 unique data with $F > 3.0\sigma(F)$. Variable-temperature magnetic susceptibility data are presented for **3** at 10.0 kG in the 5–320 K range. The μ_{eff}/molecule value rises from 9.1 μ_B at room temperature to a maximum of 9.72 μ_B at 60.0 K and then decreases to 8.95 μ_B at 5.01 K. Fitting of the data to the appropriate theoretical expression gave the following fitting parameters: J_{34} = −27.1 cm^{-1}, J_{33} = +11.1 cm^{-1}, and g = 1.95. These are similar to those for the R = Me complex (**2**) reported previously and similarly yield a well-isolated $S = {}^9/_2$ ground state. This was confirmed by variable-field magnetization studies which verified an $S = {}^9/_2$ ground state experiencing zero-field splitting (D = 0.50 cm^{-1}). The results of ^{1}H and ^{2}H NMR studies on **4–6** are presented, together with those for the 4-picoline (**7**) and 3,5-lutidine (**8**) derivatives. The observed spectra are qualitatively interpreted vis-à-vis the spin delocalization mechanisms that are operative. It is concluded that contact shifts via π-spin delocalization and dipolar shifts are both contributors to the pyridine ^{1}H and ^{2}H chemical shifts. The greater solubility of the R = aryl derivatives (except **3** and **6**) compared to R = alkyl derivatives has allowed better-resolved toluene glass EPR spectra to be obtained for complex **5** than was previously possible for the R = alkyl complexes.

Introduction

Over the last several years, we have expended a lot of time and energy in developing higher oxidation state Mn chemistry at various nuclearity levels and with exclusively or predominantly carboxylate ligation.[3-6] These studies have been stimulated by both biological modeling purposes (for example, of the tetranuclear Mn site responsible for photosynthetic water oxidation in green plants and cyanobacteria)[7] and the growing recognition that Mn aggregates have a propensity to possess ground states with large spin values.[3,8] The latter property appears to arise from the presence within the Mn_x aggregate of (i) ferromagnetic exchange interactions between at least some of the Mn ions[3,6a] and/or (ii) spin frustration effects when ≥3 Mn ions are present and arranged in an appropriate manner.[4a,6a,9]

Of relevance to both the above areas are the tetranuclear $Mn^{III}_3Mn^{IV}$ complexes possessing a distorted $[Mn_4O_3Cl]^{6+}$ cubane core. These are the only known Mn_4 species at this oxidation level and we have proposed them as potential models for one of the oxidation levels (S_2) of the water oxidation enzyme's Mn_4 site.[6,7d] In a recent report, we described in detail the syntheses and structural, spectroscopic, and magnetochemical characterization of $Mn_4O_3Cl_4(O_2CR)_3(py)_3$ (R = alkyl) and related complexes and showed that they have $S = {}^9/_2$ ground states.[6a] The results of LCAO Xα calculations that also indicate a $S = {}^9/_2$ ground state and give a detailed analysis of the mechanisms of exchange interactions in one $Mn^{III}_3Mn^{IV}O_3Cl$ complex have appeared.[6e] Unfortunately, these complexes are only sparingly soluble. It was mentioned in passing that initial attempts to prepare the $PhCO_2^-$ analogues had proven unsuccessful. We have since pursued their preparation more vigorously. There are several reasons to prepare such complexes: (i) to determine whether they would be isostructural

(1) (a) Indiana University Chemistry Department. (b) Indiana University Molecular Structure Center.
(2) University of California at San Diego.
(3) Christou, G. *Acc. Chem. Res.* **1989**, *22*, 328.
(4) (a) Libby, E.; McCusker, J. K.; Schmitt, E. A.; Folting, K.; Hendrickson, D. N.; Christou, G. *Inorg. Chem.* **1991**, *30*, 3486. (b) Bouwman, E.; Bolcar, M. A.; Libby, E.; Huffman, J. C.; Folting, K.; Christou, G. *Inorg. Chem.* **1992**, *31*, 5185.
(5) (a) Wang, S.; Tsai, H.-L.; Streib, W. E.; Christou, G.; Hendrickson, D. N. *J. Chem. Soc., Chem. Commun.* **1992**, 677. (b) Wang, S.; Huffman, J. C.; Folting, K.; Streib, W. E.; Lobkovsky, E. B.; Christou, G. *Angew. Chem., Int. Ed. Engl.* **1991**, *30*, 1672. (c) Wang, S.; Folting, K.; Streib, W. E.; Schmitt, E. A.; McCusker, J. K.; Hendrickson, D. N.; Christou, G. *Angew. Chem., Int. Ed. Engl.* **1991**, *30*, 305.
(6) (a) Hendrickson, D. N.; Christou, G.; Schmitt, E. A.; Libby, E.; Bashkin, J. S.; Wang, S.; Tsai, H.-L.; Vincent, J. B.; Boyd, P. D. W.; Huffman, J. C.; Folting, K.; Li, Q.; Streib, W. E. *J. Am. Chem. Soc.* **1992**, *114*, 2455. (b) Bashkin, J. S.; Chang, H.-R.; Streib, W. E.; Huffman, J. C.; Hendrickson, D. N.; Christou, G. *J. Am. Chem. Soc.* **1987**, *109*, 6502. (c) Li, Q.; Vincent, J. B.; Libby, E.; Chang, H.-R.; Huffman, J. C.; Boyd, P. D. W.; Christou, G.; Hendrickson, D. N. *Angew. Chem., Int. Ed. Engl.* **1988**, *27*, 1731. (d) Wang, S.; Tsai, H.-L.; Streib, W. E.; Christou, G.; Hendrickson, D. N. *J. Chem. Soc., Chem. Commun.* **1992**, 1427. (e) Schmitt, E. A.; Noodleman, L.; Baerends, E. J.; Hendrickson, D. N. *J. Am. Chem. Soc.* **1992**, *114*, 6109.
(7) See for example: (a) *Manganese Redox Enzymes*; Pecoraro, V. L., Ed.; VCH Publishers: New York, 1992. (b) Hansson, Ö.; Wydrzynski, T. *Photosynth. Res.* **1990**, *23*, 131. (c) Wieghardt, K. *Angew. Chem., Int. Ed. Engl.* **1989**, *28*, 1153. (d) Christou, G.; Vincent, J. B. *Biochim. Biophys. Acta* **1987**, *895*, 259. (e) Renger, G. *Angew. Chem., Int. Ed. Engl.* **1987**, *26*, 643.
(8) (a) Caneschi, A.; Gatteschi, D.; Laugier, J.; Ray, P.; Sessoli, R.; Zanchini, C. *J. Am. Chem. Soc.* **1988**, *110*, 2795. (b) Boyd, P. D. W.; Li, Q.; Vincent, J. B.; Folting, K.; Chang, H.-R.; Streib, W. E.; Huffman, J. C.; Chrisotu, G.; Hendrickson, D. N. *J. Am. Chem. Soc.* **1988**, *110*, 8537. (c) Caneschi, A.; Gatteschi, D.; Sessoli, R.; Barra, A. L.; Brunel, L. C.; Guillot, M. *J. Am. Chem. Soc.* **1991**, *113*, 5873. (d) Schake, A. R.; Tsai, H.-L.; DeVries, N.; Webb, R. J.; Folting, K.; Hendrickson, D. N.; Christou, G. *J. Chem. Soc., Chem. Commun.* **1992**, 181. (e) Sessoli, R.; Tsai, H.-L.; Schake, A. R.; Wang, S.; Vincent, J. B.; Folting, K.; Gatteschi, D.; Christou, G.; Hendrickson, D. N. *J. Am. Chem. Soc.* **1993**, *115*, 1804.
(9) McCusker, J. K.; Schmitt, E. A.; Hendrickson, D. N. In *Magnetic Molecular Materials*; Gatteschi, D., Kahn, O., Miller, J. S., Palacio, F., Eds.; Kluwer Academic Publishers: Boston, MA, 1991; pp 297–319.

0020-1669/93/1332-2025$04.00/0

with the alkanecarboxylate species and be isolated at the same oxidation level; (ii) to achieve more detailed spectroscopic characterization, particularly by NMR, than was previously possible, because their solubility in common organic solvents would presumably be greater; and (iii) if they are isostructural, to assess any influence of the aryl vs alkyl difference on spectroscopic and magnetochemical properties.

We herein report the successful development of synthetic procedures to prepare $[Mn_4O_3Cl]^{6+}$ complexes with arenecarboxylate ligation and describe their characterization by a number of techniques. We also describe a higher-yield procedure to prepare $[Mn_4O_3Cl_4(O_2CMe)_3(py)_3]$ than that in our previous report.[6a]

Experimental Section

Syntheses. All manipulations were performed under aerobic conditions, and all chemicals were used as received unless otherwise stated. ($O_2CC_6H_3Cl_2$ = 3,5-dichlorobenzoate; $O_2CC_6H_4F$ = 4-fluorobenzoate; $O_2CC_6H_3F_2$ = 3,5-difluorobenzoate; Me-py = 4-picoline; Me_2-py = 3,5-lutidine.) $[Mn_3O(O_2CMe)_6(py)_3](ClO_4)$ (**1**) and $[Mn_3O(O_2CMe)_6(C_5D_5N)_3](ClO_4)$ (**1a**) were available from previous work.[10] Elemental analyses were performed by Atlantic Microlab or the Microanalytical Laboratory of the University of Manchester. Metal content was determined by an EDTA titration.[11] All compounds described below were stored at −20 °C.

$[Mn_4O_3Cl_4(O_2CMe)_3(py)_3]\cdot MeCN$ (2·MeCN). To a stirred brown solution of $[Mn_3O(O_2CMe)_6(py)_3](ClO_4)$ (**1**) (0.87 g, 1.0 mmol) in MeCN (25 mL, distilled over CaH_2) was added dropwise MeCOCl (0.25 mL, 3.5 mmol). The resulting red-brown solution was left undisturbed at 5 °C for a few days. A microcrystalline precipitate was then collected by filtration in two successive crops. Each crop was washed with MeCN and EtOH[12] and dried under vacuum. The total yield was in the 55–68% range. Anal. Calcd (found) for $C_{23}H_{27}N_4O_9Cl_4Mn_4$: C, 31.94 (31.63); H, 3.15 (3.31); N, 6.48 (6.50); Mn, 25.40 (24.5). IR and NMR spectra were identical to those of the original preparation.[6a] $Mn_4O_3Cl_4(O_2CMe)_3(C_5D_5N)_3$ (**2a**) was prepared in an analogous manner from $[Mn_3O(O_2CMe)_6(C_5D_5N)_3]ClO_4$ (**1a**).

$Mn_4O_3Cl_4(O_2CC_6H_3Cl_2)_3(py)_3$ (3). A slurry of complex **2** (0.45 g, 0.52 mmol) and 3,5-dichlorobenzoic acid (0.57 g, 3.0 mmol) in PhMe (40 mL) was stirred for 2 days at ambient temperature. This gave a light brown powder and a dark brown solution. The powder was collected by filtration, washed with EtOH and Et_2O, and dried in air. The yield was 0.28 g (41%). Selected IR data (Nujol mull): 1611 (m), 1591 (m), 1553 (s), 1487 (m), 1435 (s), 1219 (m), 1071 (m), 1047 (m), 1019 (m), 895 (m), 802 (m), 781 (m), 743 (m), 689 (m), 652 (m), 613 (m), 571 (m), 511 (m), 476 (w), 438 cm^{-1} (w). An additional crop of **3** was obtained by removing the solvent under vacuum from the brown filtrate; the resulting solid was redissolved in CH_2Cl_2 (13 mL) and layered with 3:1 hexanes/Et_2O (10 mL). A dark brown crystalline material and a light brown powder formed over several days. For crystallographic characterization, the crystals were stored in the mother liquor to prevent solvent loss. The IR spectra of crystals and the original powder were identical. Anal. Calcd (found) for $C_{36}H_{24}N_3O_9Cl_{10}Mn_4$: C, 35.53 (35.27); H, 1.99 (2.25); N, 3.45 (3.27); Cl, 29.13 (29.31).

$[Mn_4O_3Cl_4(O_2CPh)_3(py)_3]\cdot H_2O$ (4·H_2O). A slurry of complex **2** (0.45 g, 0.52 mmol) and benzoic acid (0.24 g, 2.0 mmol) in PhMe (40 mL) was stirred overnight at ambient temperature. This resulted in a light brown powder and a brown solution. The solvent was removed under vacuum. The resulting solid residue was redissolved in PhMe (20 mL) and the solvent then removed again under vacuum. This step was repeated five times or until no trace of remaining bound acetate could be detected by NMR (vide infra). The solid was washed with ether and pentane and dried in the air. The yield was 0.48 g (90%). Crystalline material can be prepared by layering a CH_2Cl_2 solution of the product with pentane. Anal. Calcd (found) for $C_{36}H_{32}N_3O_{10}Cl_4Mn_4$: C, 42.05 (42.08); H, 3.14 (3.17); N, 4.12 (4.10); Cl, 13.91 (13.69); Mn, 21.56 (21.7). Selected IR data (Nujol mull): 1609 (m), 1593 (m), 1551 (s), 1534 (s), 1489 (m), 1402 (s), 1221 (m), 1071 (m), 1046 (w), 1020 (w), 758 (w), 689 (s), 650 (m), 610 (s), 563 (m), 505 (m), 475 cm^{-1} (m). $Mn_4O_3Cl_4(O_2CPh)_3(C_5D_5N)_3$ (**4a**) was prepared in an analogous manner using **2a**.

$[Mn_4O_3Cl_4(O_2CC_6H_4F)_3(py)_3]\cdot{}^1/_2H_2O$ (5·$^1/_2H_2O$) and $Mn_4O_3Cl_4(O_2CC_6H_3F_2)_3(py)_3$ (6). Complexes **5** and **6** were prepared in a manner analogous to that for **4** using 4-fluorobenzoic acid (0.28 g, 2.0 mmol) and 3,5-difluorobenzoic acid (0.32 g, 2.0 mmol), respectively. The yield for complex **5** was 0.40 g (72%). Anal. Calcd (found) for $C_{36}H_{28}N_3O_{9.5}F_3Cl_4Mn_4$: C, 40.29 (40.3); H, 2.63 (2.7); N, 3.92 (3.8); F, 5.31 (5.25); Mn, 20.48 (20.4). IR data (Nujol mull): 1605 (s), 1549 (s), 1536 (s), 1507 (m), 1485 (m), 1397 (s), 1227 (s), 1152 (s), 1071 (m), 1047 (m), 1019 (m), 860 (m), 779 (m), 691 (m), 650 (m), 643 (m), 631 (m), 615 (m), 563 (m), 502 (m), 440 cm^{-1} (w). The yield for complex **6** was 0.45 g (76%). This solid was characterized by IR and NMR only. IR data (Nujol mull): 3071 (m), 1611 (m), 1578 (s), 1559 (s), 1395 (s), 1223 (m), 1125 (s), 1073 (m), 1047 (m), 990 (s), 955 (m), 882 (m), 787 (m), 770 (m), 689 (m), 652 (w), 623 (m), 577 (s), 505 (m), 455 cm^{-1} (w).

$Mn_4O_3Cl_4(O_2CPh)_3(Me\text{-}py)_3$ (7) and $Mn_4O_3Cl_4(O_2CPh)_3(Me_2\text{-}py)_3$ (8). The following syntheses were performed under an inert atmosphere (N_2) and by using distilled PhMe (Na/benzophenone), CH_2Cl_2 (CaH_2), and hexanes (Na/benzophenone). To a stirred solution of **4a** (0.22 g, 0.20 mmol) in PhMe (40 mL) was added either 4-picoline (0.07 mL, 0.7 mmol) or 3,5-lutidine (0.09 mL, 0.8 mmol) at −77 °C for products **7** and **8**, respectively. After 1 h, the cooling bath was withdrawn and the solvent was removed under vacuum. The residue was dissolved in PhMe (10 mL), the solvent removed again under vacuum, and the solid washed with ether and hexanes. A CH_2Cl_2 solution of the product was layered with hexanes, and the resulting powder was washed with hexanes. CH_2Cl_2 was added to the solid, and the solvent was then removed under vacuum four times to reduce the amount of volatile impurities. Products were characterized by NMR only.

X-ray Crystallography and Structure Solution. Data were collected on a Picker four-circle diffractometer at −171 °C; details of the diffractometry, low-temperature facilities, and computational procedures employed by the MSC are available elsewhere.[13] The sample was known to lose solvent, so it was kept in contact with its mother liquor until a suitable crystal was chosen and transferred to the goniostat for characterization. A systematic search of a limited hemisphere of reciprocal space yielded a set of reflections with symmetry that could be indexed using a rhombohedrally-centered hexagonal lattice. The choice of space group $R\bar{3}$ was confirmed by successful solution and refinement of the structure. After standard data reduction and averaging of equivalent reflections, a unique set of 1982 observed reflections ($F > 3.0\sigma(F)$) was obtained. The structure was solved using direct methods (SHELXS-86).[14] All non-hydrogen atoms were readily located and were well-behaved except those of a disordered hexane molecule lying on a special position ($\bar{3}$ site) (Solution of the structure in noncentrosymmetric space group $R3$ led to two identical, independent molecules being located. Attempts to refine the structure proved unsatisfactory, with behavior typical of a misassigned space group. Statistical tests also strongly suggested a centrosymmetric space group.) All non-hydrogen atoms were refined anisotropically except the hexane carbon atoms, which were refined isotropically. Most hydrogen atoms were visible in a difference Fourier map phased on the non-hydrogen atoms; all hydrogens were included in fixed, idealized positions for the final stages of full-matrix least-squares refinement. All reflections were included in the refinement, but reflections having $F < 3.0\sigma(F)$ were given zero weight. The final difference Fourier map was essentially featureless, the largest peak being 0.71 e/Å^3, near the disordered hexane molecule. Final R (R_w) values are listed in Table I.

Physical Measurements. Infrared spectra (Nujol mull) were recorded on a Nicolet Model 510P spectrophotometer. ^1H NMR spectra were recorded on a Varian XL-300 spectrometer with the protio-solvent signal used as a reference. ^2H NMR spectra were recorded on a Nicolet NT-360 spectrometer with the deuterio-solvent signal used as a reference. Chemical shifts are quoted on the δ scale (downfield shifts are positive). EPR measurements were performed at X-band frequencies (9.4 GHz) on a Bruker ESP300 spectrometer with a Hewlett-Packard 5350B microwave frequency counter and an Oxford liquid He cryostat and temperature controller.

(10) Vincent, J. B.; Chang, H.-R.; Folting, K.; Huffman, J. C.; Christou, G.; Hendrickson, D. N. *J. Am. Chem. Soc.* **1987**, *109*, 5703.
(11) Vogel, A. I. *Vogel's Textbook of Quantitative Chemical Analysis*; John Wiley and Sons, Inc.: New York, 1989; pp 311–328.
(12) MeOH was later found to remove a white byproduct more efficiently.
(13) Chisholm, M. H.; Folting, K.; Huffman, J. C.; Kirkpatrick, C. C. *Inorg. Chem.* **1984**, *23*, 1021.
(14) Sheldrick, G. M. In *Crystallographic Computing 3*; Sheldrick, G. M., Krüger, C., Goddard, R., Eds.; Oxford University Press: New York, 1985; pp 175–189.

Table I. Crystallographic Data for Complex $3{\cdot}3CH_2Cl_2{\cdot}xC_6H_{14}$

formula	$C_{39}H_{30}Cl_{16}Mn_4N_3O_9$[a]	ρ_{calc}, g cm^{-3}	1.649
fw	1471.68[a]	μ, cm^{-1}	15.761
crystal system	hexagonal	octants	$\pm h,\pm k,\pm l$
space group	$R\bar{3}$	no. of total data	10 989
a, Å	19.056(4)	no. of unique data	2610
c, Å	28.271(6)	R_{merge}	0.106
V, Å^3	8888.25	no. of obsd data	1982
Z	6		($F > 3.0\sigma(F)$)
T, °C	−171	R	0.0417
radiation λ, Å	0.710 69[b]	R_w	0.0384

[a] Excluding hexane molecules. [b] Graphite monochromator.

Variable-temperature magnetic susceptibility data for powdered samples of complex **3** (restrained in Parafilm to prevent torquing) were recorded in the temperature range 5–320 K and at an applied field of 10 kG. Data were also collected in the temperature range 2–30 K at applied fields of 5–50 kG. A diamagnetic correction, estimated from Pascal's constants, was subtracted from the experimental susceptibilities to give the molar paramagnetic susceptibilities.

Results

Improved Synthesis of $Mn_4O_3Cl_4(O_2CMe)_3(py)_3$ (2). In our previous report,[6a] we described how treatment of the Mn^{III}_3 complex $[Mn_3O(O_2CR)_6(py)_3](ClO_4)$ (R = Me, Et) with (optimally) 5 equiv of the carboxylate-abstraction reagent Me_3SiCl leads to formation of the distorted cubane $Mn^{III}_3Mn^{IV}$ complexes $Mn_4O_3Cl_4(O_2CR)_3(py)_3$. The equation describing this transformation was deduced to be that shown in (1); this predicts a

$$3Mn^{III}_3O^{7+} \rightarrow Mn^{IV}Mn^{III}_3O_3^{7+} + 4Mn^{3+} + Mn^{2+} \quad (1)$$

maximum yield of 44.4% (based on total available Mn), consistent with experimental yields in the ~40% range. The reaction yield was concluded to be oxide- and carboxylate-limited, with the optimum 5:1 ratio of reactants corresponding to removal of all carboxylates except those required in the cubane product (eq 2).

$$3[Mn_3O(O_2CR)_6(py)_3]^+ + 15Me_3SiCl \rightarrow Mn_4O_3Cl_4(O_2CR)_3(py)_3 + 15Me_3SiO_2CR + 6py + 4Mn^{3+} + Mn^{2+} + 11Cl^- \quad (2)$$

It has now been found that the use of MeCOCl instead of Me_3SiCl leads to improved yields of product. Thus, treatment of $[Mn_3O(O_2CMe)_6(py)_3]^+$ with MeCOCl results in its clean conversion to $Mn_4O_3Cl_4(O_2CMe)_3(py)_3$ (**2**) with an optimum yield of 68% at a Mn_3O:MeCOCl ratio of 1:3, in contrast to the 1:5 optimum ratio in the Me_3SiCl reactions. The two systems are clearly not analogous, and we propose that eq 3 better summarizes the MeCOCl reaction system. A simplified form of eq 3 is eq 4. This suggests a maximum yield of 80% for **2**,

$$5[Mn_3O(O_2CMe)_6(py)_3]^+ + 15MeCOCl + 4H_2O \rightarrow 3Mn_4O_3Cl_4(O_2CMe)_3(py)_3 + 15(MeCO)_2O + 3Mn^{2+} + 6pyH^+MeCO_2^- + 2H^+ + 3Cl^- \quad (3)$$

$$5Mn_3O^{7+} + 4H_2O \rightarrow 3Mn_4O_3^{7+} + 3Mn^{2+} + 8H^+ \quad (4)$$

consistent with observed values. Clearly, the yield can no longer be acetate-limited, and eqs 3 and 4 also suggest incorporation of oxides from adventitious H_2O. In support of this, a 1:3 reaction was performed under anaerobic conditions employing freshly-distilled solvents, and the yield of **2** was reduced to 42%, more consistent with eq 1. In contrast, the yields of the Me_3SiCl reactions performed under anhydrous conditions under N_2 or in air using solvents as received are essentially identical. For whatever detailed mechanistic reasons, the Me_3SiCl and MeCOCl reactions thus give different yields, with the latter being the preferred reagent. Although we have not yet done so, this improved procedure could no doubt be extended to the preparation of $EtCO_2^-$ or substituted py and imidazole versions of **2**.

Incorporation of Arenecarboxylate Ligation. Initial attempts to prepare $[Mn_4O_3Cl]^{6+}$ complexes with $PhCO_2^-$ ligation involved treatment of $[Mn_3O(O_2CPh)_6(py)_3](ClO_4)$ with either Me_3SiCl or PhCOCl. In contrast to the alkanecarboxylate reactions, however, these reaction systems did not give the desired products. The analogous reactions with $Mn_3O(O_2CPh)_6(py)_2(H_2O)$ ($Mn^{II}Mn^{III}_2$) were also unsuccessful. In no case were we able to characterize the product(s) of the Me_3SiCl reactions. With PhCOCl, the Mn^{III}_3 reagent yielded a crystalline product whose analysis and IR spectrum suggest possibly a higher nuclearity product; precedents for such a possibility include (NBu^n_4)-$[Mn_8O_6Cl_6(O_2CPh)_7(H_2O)_2]$.[5c] Structural characterization of this product has yet to be accomplished. However, the $Mn^{II}Mn^{III}_2$ reagent also yielded a crystalline product, and this complex we were able to identify crystallographically as $[Mn^{III}_3O(O_2CPh)_6$-$(py)_3]_2[Mn^{II}Cl_4]$, containing separate anions and cations. It thus appears for all the above reactions that even if the desired $[Mn_4O_3Cl]^{6+}$ species were formed and were present in solution, they were not preferentially crystallizing out as had the alkanecarboxylate systems, perhaps due to greater solubility. We thus resorted to an alternative approach, ligand exchange of the AcO^- groups of preformed **2** with excess $PhCO_2H$.

Ligand substitution of AcO^- with $PhCO_2^-$ had proven, in several cases,[4a,8e,15] to be a clean and efficient way of altering the peripheral carboxylate environment around Mn_x aggregates without structural changes to the core. Treatment of complex **2** with PhCOOH (6 equiv) in MeCN or CH_2Cl_2, however, gave mixtures of products that NMR suggested to be mixed $AcO^-/PhCO_2^-$ cubanes (vide infra). This is in contrast, for example, to the corresponding reactions with the Mn^{III}_4 complexes possessing the "butterfly" $[Mn_4O_2]^{8+}$ core that readily undergo complete substitution under the same conditions. We suspected the origin of the problem to be possibly both thermodynamic (equilibrium positions not totally toward the fully substituted species) and kinetic (relative substitutional lability of d^3 Mn^{IV} (cf. Cr^{III})). The following general procedure was thus employed: A slurry of **2** in toluene was treated with ArCOOH (4–6 equiv; Ar = 3,5-Cl_2-Ph (**3**), Ph (**4**), 4-F-Ph (**5**), or 3,5-F_2-Ph (**6**)) and the mixture stirred for 12–24 h. To ensure removal of all AcO^- groups, the solvent was removed under vacuum (acetic acid forms a 28%:72% azeotrope with toluene) and the residue redissolved in toluene. The evaporation/redissolution step was repeated until NMR indicated essentially complete loss of the bound AcO^- signal. For complex **3**, the evaporation step was found to be unnecessary, the low solubility of **3** and relatively high acidity of this acid presumably helping to drive the reaction to completion.

As had been hoped, the arenecarboxylate complexes have significantly enhanced solubility (except for **3** and **6**) and are quite soluble, for example, in toluene. This also allowed the py groups of complex **4** to be replaced with 4-picoline (**7**) or 3,5-lutidine (**8**) by a ligand substitution procedure in this solvent; complexes **7** and **8** were required merely to assist in the NMR studies, and their preparations in large amounts or high purities were therefore not pursued.

Description of Structure. An ORTEP projection of complex **3** is shown in Figure 1. Selected atomic coordinates and interatomic distances and angles are listed in Tables II and III, respectively. Complex **3** crystallizes in hexagonal space group $R\bar{3}$ with the Mn_4 molecule lying on a 3-fold rotation axis passing through Mn(1) and Cl(3). The molecule has no other imposed or virtual symmetry elements and thus has C_3 symmetry. There are also CH_2Cl_2 and hexane molecules in the unit cell; these are

(15) Vincent, J. B.; Christmas, C.; Chang, H.-R.; Li, Q.; Boyd, P. D. W.; Huffman, J. C.; Hendrickson, D. N.; Christou, G. *J. Am. Chem. Soc.* **1989**, *111*, 2086.

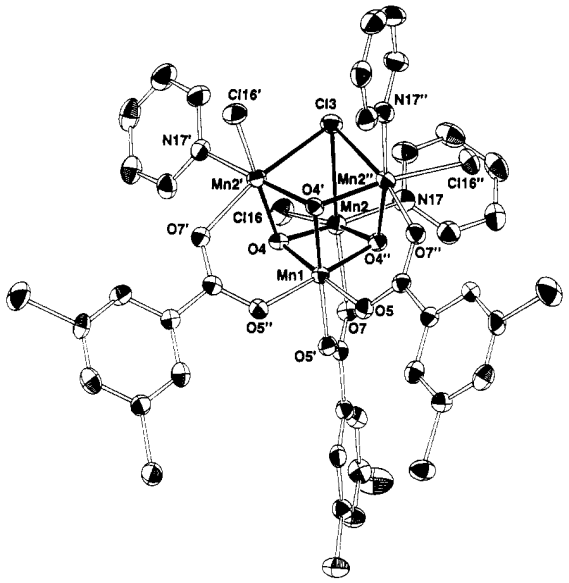

Figure 1. ORTEP plot for complex **3** at the 50% probability level. Primed and unprimed atoms are related by the crystallographic C_3 axis.

Table II. Selected Fractional Coordinates ($\times 10^4$)[a] and Isotropic Thermal Parameters ($\times 10$) for Complex $3 \cdot 3CH_2Cl_2 \cdot xC_6H_{14}$

atom	x	y	z	B_{iso}, Å^2
Mn(1)	6667*	3333*	9508.1(5)	16
Mn(2)	5542(1)	2609.1(5)	10242.2(3)	18
Cl(3)	6667*	3333*	10892(1)	22
O(4)	6344(2)	2465(2)	9919(1)	17
O(5)	7030(2)	4264(2)	9088(1)	19
C(6)	4993(3)	2350(3)	9223(2)	17
O(7)	4761(2)	2229(2)	9640(1)	20
C(8)	4380(3)	1981(3)	8839(2)	18
C(9)	4602(3)	2114(3)	8366(2)	21
C(10)	4011(3)	1758(3)	8023(2)	21
C(11)	3203(4)	1273(4)	8147(2)	27
C(12)	3000(3)	1155(3)	8615(2)	24
C(13)	3571(3)	1504(3)	8967(2)	22
Cl(14)	4276(1)	1939(1)	7433.3(5)	28
Cl(15)	1983(1)	552(1)	8772(1)	43
Cl(16)	4929(1)	1356(1)	10536(1)	28
N(17)	4810(3)	2925(3)	10611(2)	22
C(18)	4701(4)	2803(4)	11079(2)	28
C(19)	4250(4)	3046(4)	11332(2)	35
C(20)	3904(4)	3441(4)	11101(2)	34
C(21)	4009(4)	3558(4)	10619(2)	28
C(22)	4463(3)	3293(4)	10385(2)	26

[a] Parameters with an asterisk were not varied.

well-separated from the Mn_4 molecule and will not be further discussed. The $[Mn_4O_3Cl]^{6+}$ core of **3** is essentially superimposable on those of the alkanecarboxylate complexes, showing very little structural effect of the alkyl vs aryl difference. Atom Mn(1) is clearly identifiable as the Mn^{IV} center, and the other Mn atoms are Jahn–Teller distorted Mn^{III} centers; the μ_3-Cl^- ion Cl(3) lies on the JT elongation axes of all three Mn^{III} atoms.

With respect to the objectives of the work outlined in the Introduction, it is clear that arenecarboxylate cubanes are indeed attainable and stable at the same oxidation level as the alkanecarboxylate species and that they possess nearly structural congruency with the latter. This is emphasized by the structural comparison of **3** with **2** in Table IV. Of relevance to magnetochemical comparisons between the two types (vide infra) are the structural parameters involving the bridging O^{2-} ions (O_b) of the core, for these are the prime mediators of the exchange interactions between the Mn centers. Of particular importance to the latter are the $Mn^{III}\cdots Mn^{IV}$, Mn^{III}–O_b, Mn^{IV}–O_b, and Mn^{III}–O_b–Mn^{IV} parameters; of these, only the first has a difference that can be considered significant using the usual 3σ criterion, but this difference is nevertheless very small. Even the Mn^{III}–O_c and

Table III. Selected Interatomic Distances (Å) and Angles (deg) for Complex $3 \cdot 3CH_2Cl_2 \cdot xC_6H_{14}$

a. Distances

Mn(1)···Mn(2)	2.802(1)	Mn(2)···Mn(2′)	3.260(1)
Mn(1)–O(4)	1.857(3)	Mn(1)–O(5)	1.951(3)
Mn(2)–Cl(3)	2.629(2)	Mn(2)–Cl(16)	2.229(2)
Mn(2)–O(4)	1.915(4)	Mn(2)–O(4″)	1.958(4)
Mn(2)–O(7)	2.134(4)	Mn(2)–N(17)	2.056(5)

b. Angles

Mn(1)–O(4)–Mn(2)	95.93(16)	Mn(1)–O(4)–Mn(2′)	94.48(16)
Mn(2)–O(4)–Mn(2′)	114.65(17)	Mn(2)–Cl(3)–Mn(2′)	76.63(6)
O(4)–Mn(1)–O(4′)	85.02(16)	O(4)–Mn(1)–O(5′)	94.74(14)
O(4)–Mn(1)–O(5″)	93.44(15)	O(4)–Mn(1)–O(5)	178.46(16)
O(5)–Mn(1)–O(5′)	86.79(16)	O(4)–Mn(2)–O(4″)	80.77(20)
O(4)–Mn(2)–O(7)	92.41(14)	O(4″)–Mn(2)–O(7)	85.18(14)
O(4)–Mn(2)–N(17)	171.97(17)	O(4″)–Mn(2)–N(17)	93.33(16)
O(7)–Mn(2)–N(17)	92.52(16)	Cl(3)–Mn(2)–Cl(16)	98.90(6)
Cl(3)–Mn(2)–O(4)	84.76(11)	Cl(3)–Mn(2)–O(4″)	83.94(11)
Cl(3)–Mn(2)–O(7)	169.07(11)	Cl(3)–Mn(2)–N(17)	89.22(13)
Cl(16)–Mn(2)–O(4)	92.98(11)	Cl(16)–Mn(2)–O(4″)	172.90(11)
Cl(16)–Mn(2)–O(7)	91.77(11)	Cl(16)–Mn(2)–N(17)	93.21(14)

Table IV. Comparison of Selected Structural Parameters (Å, deg) for **2** and **3**

parameter	**2**	**3**
$Mn^{IV}\cdots Mn^{III}$	2.815(2)	2.802(1)
$Mn^{III}\cdots Mn^{III}$	3.269(2)	3.260(1)
Mn^{IV}–O_b	1.865(3)	1.857(3)
Mn^{IV}–O_c	1.950(3)	1.951(3)
Mn^{III}–Cl_b	2.627(2)	2.629(2)
Mn^{III}–O_b[a]	1.922(3)	1.915(4)
Mn^{III}–O_b[b]	1.966(3)	1.958(4)
Mn^{III}–O_c	2.146(3)	2.134(4)
Mn^{IV}–O_b–Mn^{III}[a]	96.00(15)	95.93(16)
Mn^{IV}–O_b–Mn^{III}[b]	94.51(15)	94.48(16)
Mn^{III}–O_b–Mn^{III}	114.48(17)	114.65(17)

[a] Bond trans to pyridine. [b] Bond trans to Cl.

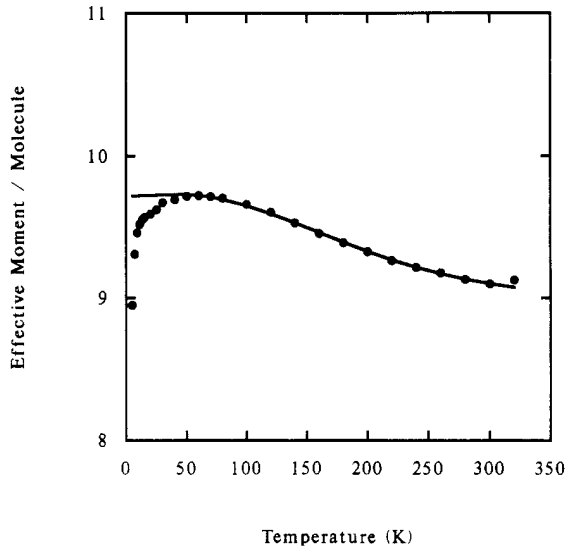

Figure 2. Plot of the effective magnetic moment (μ_{eff}) per molecule of **3** vs temperature. The solid line results from fitting the data to the theoretical model. See text for fitting parameters.

Mn^{IV}–O_c (O_c = carboxylate oxygen) bond lengths, which might logically be expected to most noticeably reflect the carboxylate variation, are indistinguishably different in **2** and **3**.

Magnetochemical Studies. Variable-temperature magnetic susceptibility measurements were performed for powdered samples restrained in Parafilm to prevent torquing. Since the crystal structure was obtained for **3**, this was the complex chosen for magnetochemical studies. A plot is shown in Figure 2 of effective magnetic moment, μ_{eff}, per molecule vs temperature for **3** measured in a 10.0-kG applied field. The μ_{eff} value slowly rises from 9.10 μ_B at room temperature to a maximum of 9.72 μ_B at

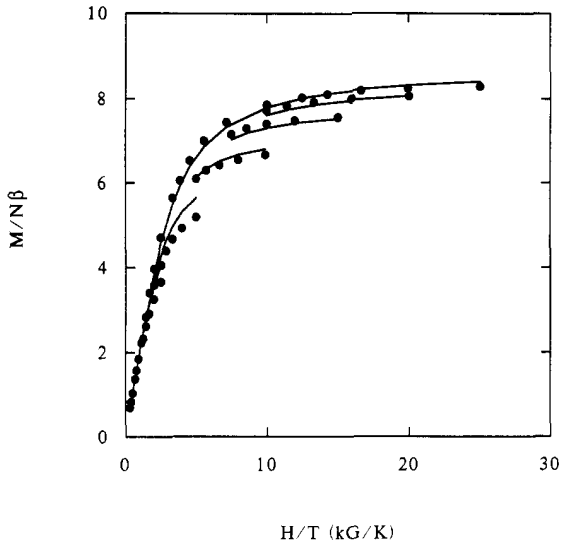

Figure 3. Plot of the reduced magnetization, $M/N\beta$, vs H/T for a polycrystalline sample of $Mn_4O_3Cl_4(O_2CC_6H_3Cl_2)_3(py)_3$ (**3**) restrained in Parafilm. The solid lines represent a calculated best fit employing the spin Hamiltonian matrix for an $S = {}^9/_2$ state experiencing axial zero-field splitting and Zeeman effects, and employing a matrix diagonalization approach.

60.0 K and then slowly decreases to 8.95 μ_B at 5.01 K (data available in supplementary material). These μ_{eff} values are comparable to those for the alkanecarboxylate complexes described previously and similarly suggest an $S = {}^9/_2$ ground state for **3**, for which the spin-only μ_{eff} value should be 9.94 μ_B.

The data in Figure 2 were least-squares-fit to the theoretical molar susceptibility vs temperature expression derived previously[6a] for a $Mn^{IV}Mn^{III}_3$ pyramid of C_3 symmetry. The data were fit only in the 60–320 K range because at temperatures below 60 K the effects of Zeeman and zero-field interactions are felt. There are three fitting variables: J_{34} and J_{33} that gauge the Mn^{III}···Mn^{IV} and Mn^{III}···Mn^{III} interactions, respectively, and an average g value for the Zeeman interaction. (The TIP term was held constant at 800 × 10^{-6} emu). The best fitting parameters were found to be $J_{34} = -27.1$ cm^{-1}, $J_{33} = +11.1$ cm^{-1}, and $g = 1.95$ cm^{-1}. The corresponding values in the same order for **2**·4MeCN, $(H_2Im)_2[Mn_4O_3Cl_6(O_2CMe)_3(HIm)]$·MeCN, and $Mn_4O_3Cl_4(O_2CEt)_3(py)_3]$·4MeCN are (–23.1, +11.3, 1.86), (–30.3, +11.1, 1.92), and (–20.8, +8.6, 2.00), respectively. The fitting parameters for **3** are thus very similar to those for the alkanecarboxylate complexes, and they similarly yield an $S = {}^9/_2$ ground state that is well isolated from the first and second excited states, which are $S = {}^7/_2$ and $S = {}^{11}/_2$ at 214.5 and 298.1 cm^{-1}, respectively, from the $S = {}^9/_2$ ground state. The decrease in μ_{eff} above 60.0 K is due to increasing population of the $S = {}^7/_2$ excited state. The sensitivity of the above fit of data to J_{33} and J_{34} parameters was examined by generating a contour plot (available in the supplementary material) showing the relative error of fitting in the J_{33}/J_{34} parameter space. There is only one minimum in the $-20 \le J_{33} \le 40$ cm^{-1} and $-60 \le J_{34} \le 0$ cm^{-1} region. While the J_{33} parameter is somewhat better determined, both of these parameters are well determined.

The above analysis of the magnetic susceptibility vs temperature behavior at 10.0 kG does not account for the low-temperature behavior which is due to zero-field splitting and Zeeman interactions. We therefore decided to investigate the magnetic field dependence of the magnetization of complex **3**. Magnetization data were collected at 5.00, 10.0, 20.0, 30.0, 40.0, and 50.0 kG in the 2–30 K range. The results are displayed in Figure 3, where reduced magnetization $M/N\beta$ (N = Avogadro's number, β = Bohr magneton) vs H/T plots are shown. Complex **3** has a well-separated $S = {}^9/_2$ ground state, and at temperatures where this is the only state populated, the high-field $M/N\beta$ data should saturate at 9.00. It can be seen that $M/N\beta$ saturates at 8.4 and that the isofield lines do not superimpose; this latter fact is attributed to zero-field splitting of the $S = {}^9/_2$ state.

Table V. Hydrogen NMR Data for Complexes **2** and **4–8**[a]

		O_2CR			py		
complex	nucleus	*o*	*m*	*p*	*o*	*m*	*p*
2[b]	^{1}H	44.6 (acetate)			n.o.	–3.6	–53.4
2a[c]	^{2}H				–100.8	–3.9	–52.5
4	^{1}H	8.8	15.2	7.8	n.o.	–3.7	–53.8
4a[d]	^{2}H				–101.5	–3.9	–52.6
5[b]	^{1}H	9.6	14.5		n.o.	–3.2	–53.4
6	^{1}H	~10.1		8.7	n.o.	–4.6	–54.7
7	^{1}H	8.7	15.1	7.7	n.o.	–3.8	(63.5)[e]
8	^{1}H	8.7	15.1	7.7	n.o.	(–19.2)[e]	–53.9

[a] Chemical shifts (±0.1) are in ppm vs TMS at ~23 °C; spectra recorded on CD_2Cl_2 or CH_2Cl_2 solutions unless otherwise indicated. n.o. = not observed; *o* = ortho; *m* = meta; *p* = para. [b] $CDCl_3$ solution. [c] Complex **2a** is $[Mn_4O_3Cl_4(O_2CMe)_3(C_5D_5N)_3]$. [d] Complex **4a** is $[Mn_4O_3Cl_4(O_2CPh)_3(C_5D_5N)_3]$. [e] Numbers in parentheses refer to Me protons at that ring position.

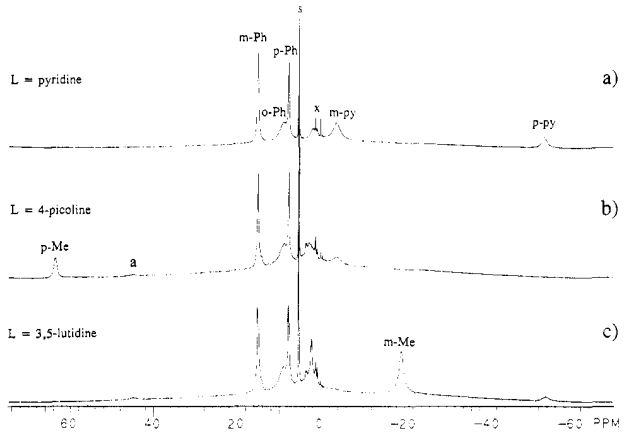

Figure 4. Proton NMR spectra in CD_2Cl_2 for complexes **4** (a), **7** (b), and **8** (c), which contain the indicated pyridine derivative (L). s = solvent $CDHCl_2$ impurity; peaks marked x include lattice solvent and free-ligand impurities; a = residual AcO^- impurity in **7** and **8**.

The experimental variable-field magnetization data were fit using the equations and procedures described elsewhere,[6a] and the solid lines in Figure 3 show the results of this fit. A full-matrix diagonalization approach was used where the spin Hamiltonian matrix for an isolated $S = {}^9/_2$ state incorporated both axial zero-field splitting ($D\hat{S}_z^2$) and isotropic Zeeman interactions. The fitting parameters are $D = +0.50$ cm^{-1} and $g = 1.98$, where the lines in Figure 3 illustrate this fit. The corresponding values for **2** were $D = +0.32$ cm^{-1} and $g = 1.94$. The obtained values of the zero-field splitting parameter D are thus slightly different for **3** vs **2** (although it should be added that fitting of susceptibility data does not provide the most accurate means of determining D values). At high-field, the $M_s = -{}^9/_2$ component of the $S = {}^9/_2$ manifold is the ground state, and at low temperature and 50.0 kG, the $M/N\beta$ saturation value approaches 9.0. The overall conclusion from the field dependence of the magnetization is that an $S = {}^9/_2$ ground state is confirmed and that it experiences zero-field splitting.

^{1}H and ^{2}H NMR Studies. Preliminary NMR studies reported previously on the alkanecarboxylate cubanes have been extended to include the arenecarboxylate complexes. Additional studies on complex **2** have also been performed. Chemical shift data for complexes **2** and **4–8** are collected in Table V. Due to its low solubility, complex **3** was omitted from this study. In Figure 4 are shown the ^{1}H spectra for **4**, **7**, and **8**. The two observable py resonances in the spectrum of **4** at –3.7 (*m*) and –53.8 ppm (*p*) are at positions essentially identical to those for complex **2**. As was previously found for **2**, the spectra of **4**, **5** (not shown), **7**, and **8** show no sign of the resonance for the py *o*-proton. Locating

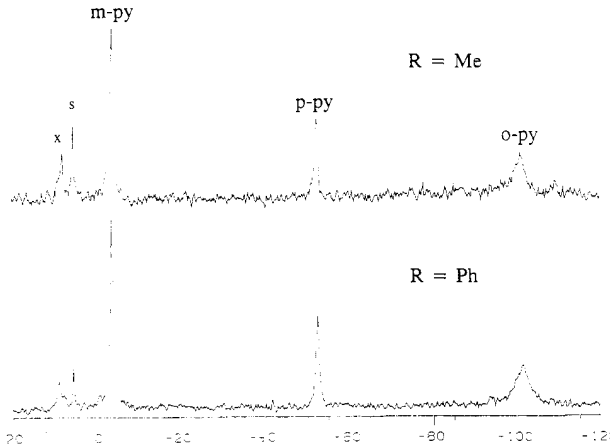

Figure 5. Deuterium NMR spectra in CH_2Cl_2 for complexes **2a** (top) and **4a** (bottom). s = solvent $CDHCl_2$ impurity; x = free-ligand impurity.

this resonance was considered essential for gaining insights into the spin delocalization mechanisms contributing to the observed paramagnetic shifts, and further studies employing ^2H NMR were therefore carried out. In theory, ^2H NMR line widths can be anything up to 42 times smaller than corresponding ^1H line widths ($\gamma_H^2/\gamma_D^2 = 42.4$, where γ is the magnetogyric ratio),[16] allowing very broadened peaks to be observed. The ^2H spectra for **2a** and **4a** are shown in Figure 5, and a broad resonance assignable to the py *o*-deuteron is clearly visible at ca. −100 ppm. Even with the resonance position of the *o*-hydrogen identified, close inspection of that region in the ^1H spectrum failed to reveal a recognizable peak, supporting our previous conclusion that this resonance was relaxation-broadened beyond detection. Proton resonances were experimentally found to be broader by roughly a factor of 10 than the corresponding deuterium resonances.

Consideration of all the NMR data in Table V and Figures 4 and 5 leads us to propose the following qualitative rationalization of the observed paramagnetic shifts. The high-spin d^4 Mn^{III} centers have their JT elongation axes directed toward the μ_3-Cl^- ion. Taking this direction as the *z* axis, the d_{z^2} orbital will be singly-occupied and the $d_{x^2-y^2}$ orbital directed toward the py groups will be empty. Thus, the contact shift contributions to the observed paramagnetic shifts of the py hydrogens should, to first order, be only via a π-spin-delocalization mechanism involving the py π system and the Mn d_π orbitals. Parallel spin at the Mn^{III} ions should lead to parallel spin at the *o*- and *p*-carbon atoms resulting in antiparallel spin at the *o*- and *p*-hydrogen nuclei and resultant upfield shifts; in contrast, the *m*-hydrogen should experience a downfield shift from spin-polarization effects. This alternating sign of the contact shifts at the *o*, *m*, and *p* positions is a telltale sign of the π-spin-delocalization mechanism.[17] However, since the *m*-hydrogen is in fact not appearing downfield of its diamagnetic position but slightly upfield, we suggest that an upfield dipolar (pseudocontact) shift of all resonances is also occurring; a significant dipolar shift contribution should be expected, given the d^4 electronic configuration of Mn^{III} and the resulting anisotropic electron distribution. Thus, the two main contributions to the observed shifts are proposed to be an alternating upfield–downfield–upfield contact shift contribution and an upfield dipolar shift contribution, the latter having the familiar r^{-3} dependence where *r* is the distance of the resonating hydrogen from the paramagnetic center.[18] The dipolar shift's distance dependence would also rationalize the factor of ~2 difference between the paramagnetic shifts of the *o*- and *p*-hydrogens. Contact shifts due to the π-delocalization mechanism tend not to attenuate dramatically with *r*,[17] and the *o*- and *p*-hydrogen shifts might thus have been expected to be more comparable in the absence of a second contribution to the shifts; i.e., the distinctly greater shift of the *o*-hydrogen is due to a significantly greater dipolar shift due to its close proximity (~3 Å in the solid-state structure) to the Mn^{III} ion.

Confirmation of a π-spin-delocalization contribution to the py paramagnetic shifts comes from consideration of the spectra of **7** and **8** in Figure 4. The 4-Me resonance of **7** is shifted downfield (+63.5 ppm) in dramatic contrast to the upfield shift of the *p*-H of **4**. The alternation in sign of H vs Me shifts at a given ring position is strong support for π spin delocalization. In fact, for these groups with their large distance (>7.8 Å) from the paramagnetic center, the π-delocalization mechanism is likely to be the dominant shift mechanism. Similarly, the 3,5-Me groups of complex **8** are shifted further upfield (−19.2 vs −3.7 ppm in **4**). This is informative and supports a downfield contribution from π delocalization to the *m*-H shift in **4** that is now an upfield shift for the *m*-Me groups; i.e., the contact and dipolar shifts are now *both* upfield.

In contrast to the py resonances, the $PhCO_2^-$ resonances of **4**, **7**, and **8** are considerably less paramagnetically shifted. The assignments were based on relative line widths and substitution at the *p*- or *m*-protons with fluoride (**5** and **6**, respectively). Consideration of the structure of **4** suggests π spin delocalization should again be contributing (overlap of Mn d_π orbitals with the carboxyl π system); however, a σ-delocalization mechanism should also be operative (the d_{z^2} orbitals are directed toward the carboxylate ligands). The greater distances between protons and Mn centers suggest decreased shifts from dipolar contributions and significantly attenuated contact shifts. The magnitudes of paramagnetic shifts (Figure 4 and Table V) are consistent with this. The pattern of shifts is indicative of the alternation from the expected π-delocalization mechanism. The *p*-H is essentially at its diamagnetic position, however, and the corresponding *p*-methylbenzoate complex has the *p*-Me resonance (2.47 ppm) insignificantly shifted from the free-ligand value (2.45 ppm). Perhaps the safest conclusion to be made is that the shifts of the arenecarboxylate resonances are relatively small and it is difficult to gauge the contributions from possible spin-delocalization mechanisms.

A study has been performed of the temperature dependence of the ^1H and ^2H NMR spectra of complexes **4** and **4a**, respectively. A plot of the variation in the ^2H paramagnetic shifts with temperature for the resonances of the py ^2H atoms of **4a** is shown in Figure 6; a similar plot for the ^1H atoms of **4** is available in the supplementary material. The main observation in Figure 6 is the dramatic increase in the paramagnetic shift of the py *o* and *p* resonances, particularly the former, which are accompanied by significant broadening. The shifts increase by approximately a factor of 2 over a ~100 K range, and all show Curie-like behavior; i.e., they decrease with increasing temperature. The benzoate ^1H resonances of **4** also show Curie-like temperature dependence and a much smaller variation in absolute shift with temperature. The *m*-H and *p*-H paramagnetic shifts vary from 7.8 and 0.2, respectively, at 293 K to 17.8 and 3.0 at 193 K; the *o*-H resonance is poorly resolved from the *p*-H resonance over most of this temperature range. Further investigations of the temperature dependence of the NMR resonances and the relative contribution of contact vs dipolar mechanisms will be the subject of a future report based on work currently in progress.

EPR and Electrochemistry. The greater solubility of arenecarboxylate complexes (except **3** and **6**) allows more detailed electrochemical studies than previously possible. Unfortunately, however, only irreversible features were observed in both anodic

(16) (a) Holm, R. H.; Hawkins, C. J. In *NMR of Paramagnetic Molecules*; Lamar, G. N., Horrocks, W. D., Jr.; Holm, R. H., Eds.; Academic Press: New York, 1973; pp 287–289, 568. (b) Johnson, A.; Everett, G. W. *J. Am. Chem. Soc.* **1972**, *94*, 1419.

(17) Horrocks, W. D., Jr. In *NMR of Paramagnetic Molecules*; Lamar, G. N., Horrocks, W. D., Jr.; Holm, R. H., Eds.; Academic Press: New York, 1973; pp 159–161.

(18) Jesson, J. P. In ref 17, pp 16–18.

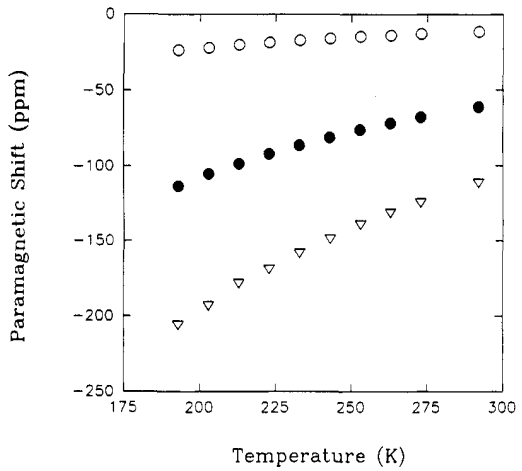

Figure 6. Temperature dependence of the paramagnetic shifts for the deuterons of complex **4a** emphasizing the Curie-like dependence for all three py resonances: ○ = *m*; ● = *p*; ▽ = *o*.

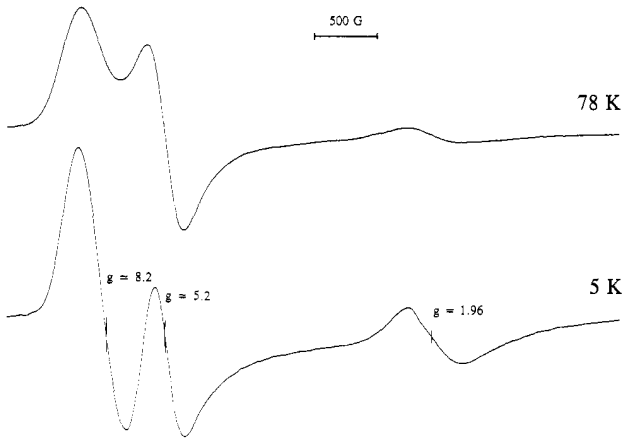

Figure 7. Toluene glass X-band EPR spectra of complex **4** at 5 and 78 K.

and cathodic scans for **4**; the same behavior was previously observed for **2**. This is in contrast to the reversible electrochemical processes recently reported for the related cubane complexes $Mn_4O_3X(O_2CMe)_3(dbm)_3$ (X = Cl, Br; dbmH = dibenzoylmethane).[6d] It is clear that the peripheral ligation can *greatly* influence the electrochemical behavior exhibited by these $[Mn_4O_3Cl]$ complexes.

The greater solubility of most of the present complexes in toluene has allowed improved EPR spectra to be obtained vis-à-vis signal strength and resolution, the latter being significantly improved by the good glassing properties of frozen toluene. The spectra for complex **4** in a toluene glass at 5 and 78 K are shown in Figure 7. The 78 K spectrum looks very similar to that of $Mn_4O_3Cl_4(O_2CEt)_3(py)_3$ (a slightly more soluble version of **2**) reported previously, in both overall appearance and the measured *g* values.[6a] Whereas EPR spectra of the $EtCO_2^-$ cubane retain the same appearance as the temperature is decreased, it can clearly be seen in Figure 7 that the resolution in the spectrum of **4** dramatically improves and the two low-field signals are consequently resolved, allowing determination of the lower-field *g* value of 8.2. No evidence for additional weaker features is seen at 5 K. Although loss of resolution and apparent signal intensity results on raising the temperature to 78 K, it is evident that the spectrum is otherwise unchanged; this is consistent with the $S = {}^9/_2$ ground state being the predominantly populated state; i.e., little population of the $S = {}^7/_2$ and $S = {}^{11}/_2$ excited states has occured at this temperature.

Discussion

Although not as straightforward as we had originally anticipated, synthetic procedures to prepare arenecarboxylate cubanes have now been successfully developed, albeit ones that require prior formation of the corresponding alkanecarboxylate derivatives; however, the improved procedure for **2** makes the latter less of an irritation. Once again, ligand substitution has proven an efficient means to alter the peripheral ligation around a Mn/O core without major changes to the latter.

With reference to the stated objectives of this work, several conclusions can be drawn. First, the arenecarboxylate species do indeed possess the same structure and are isolated at the same oxidation level. While this is not surprising with hindsight, early difficulties in their preparation had made us wonder whether the weaker-donor arenecarboxylates were perhaps incapable of stabilizing the $[Mn_4O_3Cl]^{6+}$ core. Second, the magnetic exchange interactions between the constituent Mn centers are essentially unaffected by carboxylate variation. This completes our study of the variation of these interactions in $Mn_4O_3Cl_4(O_2CR)_3(py)_3$ complexes as a function of carboxylate; a significant range of carboxylates has now been employed in this and previous work with little change in obtained values. Clearly, this supports the dominance of the oxide bridges as mediators of the exchange interactions. All products consequently have $S = {}^9/_2$ ground states well-isolated from the first excited state. We have described in detail elsewhere that spin-frustration effects are present within the $[Mn_4O_3Cl]^{6+}$ core and that the observed electronic structure and $S = {}^9/_2$ ground state depend on the relative magnitude of the J_{33} and J_{34} exchange parameters.[6a]

The most beneficial impact of arenecarboxylate incorporation is improved solubility, including in solvents such as toluene, which has allowed good EPR and NMR data to be accumulated. This also makes feasible a future exploration of the reactivity characteristics of these cubanes in homogeneous solution, particularly reactions that are relevant to modeling the photosynthetic water oxidation process.[19]

Future studies with $[Mn_4O_3Cl]^{6+}$ include the investigation of the structural and electronic consequences of the introduction of chelating ligands in place of Cl^-/py at the Mn^{III} positions and perturbations to the core (for example, Br^--for-Cl^- substitution). Initial results have already been communicated,[6d] and further studies are in progress.

Acknowledgment. This work was supported by NIH Grants GM39083 (to G.C.) and HL13652 (to D.N.H.).

Supplementary Material Available: A textural presentation of the data collection and solution of the structure for **3**, tables of crystallographic data, fractional coordinates, thermal parameters, and bond distances and angles for **3**, additional stereo diagrams of **3**, tables of effective magnetic moment versus temperature for **3** at 10.0 kG and reduced magnetization versus H/T for **3** at various fields, a figure showing a contour plot of relative error of fitting the 10.0-kG data in the J_{33}/J_{34} parameter space, and a plot of ^1H NMR paramagnetic shifts vs T for **4** (16 pages). Ordering information is given on any current masthead page.

(19) Reactions such as chemical and/or electrochemical oxidation in the presence of water, protonation of bridging oxides, etc.